Special Feature: Novel Catalytic Approach

Research Report

Mesoporous Iron-based Oxides for Clean Air: Nanoparticle-assembled Mesostructured Ferrihydrite as an Ozone Removal Catalyst

Kenichirou Suzuki

Report received on Jan. 26, 2016

ABSTRACT Environmentally compatible, readily available Fe-based oxides of the 2-line ferrihydrite (Fh) phase with mesoporous structures were prepared, and their performance was assessed in air purification applications. A template-assisted synthesis route was adopted to produce mesoporous 2-line ferrihydrite (M2LFh) in a stable form. The prepared M2LFh was thoroughly characterized and its ozone (O_3) removal ability was measured. We compared the O_3 decomposition activity of a wide variety of materials under similar experimental conditions, including several Fe-based oxides, noble-metal-supported catalysts, microporous and mesoporous oxides, and commercial O_3 decomposition catalysts. The highest activity among these materials was that of M2LFh at room temperature. Furthermore, fundamental aspects of the structure-property relationship of M2LFh were determined through various physicochemical characterization techniques such as X-ray diffraction (XRD), N_2 adsorption, transmission electron microscopy (TEM), X-ray absorption studies, and density functional theory (DFT) calculations. The presence of Fh nanoparticles in the disordered, mesostructured Fe oxide had a significant effect on the bulk and surface structure of the material and its activity. The high O_3 removal activity of M2LFh was due to the abundantly available unsaturated surface Fe sites (*tri*- and *tetra*-coordinated sites) with less oxygen packing around them and the presence of isolated FeO_x species. The present catalyst system represents the first example of a unique, biocompatible, and cost-effective catalyst system for O_3 removal that is active at room temperature.

KEYWORDS Ferrihydrite, Mesoporous Materials, Ozone, Enviromental Catalysts, XAFS, Density functional calculation

1. Introduction

Photochemical smog and the smog associated with air pollutants such as ozone (O_3), known as ground-level O_3, and other oxidation products (aldehydes, peroxyacetyl nitrate, etc.) in indoor and outdoor atmospheres[1] have raised severe ecological concerns. Such pollutants cause serious health problems, and their presence in the troposphere, particularly O_3, disrupts plant growth and thus affects agricultural production and ecological balance.[2] Although atmospheric pollutants such as volatile organic compounds (VOCs) and NO_x are the major causes of photochemical smog and ground-level O_3,[1] the rapid and irreversible chemical changes caused by the latter[1a] accentuate the necessity of developing functional materials for removing these harmful pollutants from air through an enhanced adsorption and catalytic process.[3] In contrast to traditional amelioration methods such as adsorption by activated carbon, the abatement of trace pollutants from air using mesoporous transition metal oxides as dual functional catalysts in an enhanced adsorption-decomposition process is an effective and versatile approach to improving both indoor and outdoor air quality.[4] The superior performance of mesoporous transition metal oxides for VOC removal[4] encouraged us to focus on developing more ecofriendly and cost-effective Fe-based porous materials that show high activity and adsorption capacity for air purification, both indoors and out. To treat a harmful and highly reactive pollutant, like O_3 in particular, a rapid catalyst response is needed, preferably operating at room temperature (RT).

The materials previously explored for eliminating O_3 in several indoor- and outdoor-based technology applications are varied, and include activated carbon or metal(or oxide)-containing activated

carbon, noble-metal-supported catalysts, and a variety of transition metal oxides.[5-8] The most active O_3 decomposition catalysts (e.g., MnO_2,[5] noble-metal-supported catalysts) have at least one drawback. For example, they must be deposited on metal oxides with high surface areas and/or promoted with organic additives to enhance the surface area and activity; they require the use of expensive metal components; or they exhibit relatively low environmental compatibility and poor flexibility for use in other catalytic systems. Thus, there is a strong incentive to identify a unique catalyst material that is highly active, environmentally friendly, and does not use expensive noble metals and/or byproduct-forming organic additives. This prompted us to look for highly active and environmentally compatible candidates, preferably from the most abundant transition metal category of Fe-based materials.

Among the Fe oxides and oxyhydroxides, ferrihydrite (Fh) has been the subject of voluminous studies.[9-13] The interest is due to its high reactivity, large adsorptive capacity for a number of inorganic components, ambiguous structural aspects, geographic distribution, natural sequestration ability, and practical utility in several industrial processes,[9-12] including coal liquefaction, metallurgical processing, toxic ion removal, and wastewater treatment. The poorly crystalline 2-line ferrihydrite (2LFh) and the relatively more ordered 6-line ferrihydrite, referring to two and six broad X-ray diffraction peaks, respectively, are the most common in this category.[11] Its high surface area with several coordinatively unsaturated Fe sites on the particle surface makes Fh an excellent candidate for adsorption. Despite such interesting properties and utility, conventionally synthesized Fh, which is usually precipitated from an aqueous solution of an Fe salt by treatment with a suitable base such as alkali hydroxides or ammonia solution, is perceived to be limited in its use for the elimination of organic contaminants. This is mainly because the closely packed physical characteristics and the surface hydration layer slow the diffusion of contaminant gas molecules into the surface Fe active sites, thereby slowing the rates of adsorption and catalysis.[11,14] Although partial dehydroxylation by heating would expose the surface active sites and tend to improve their adsorption ability, at elevated temperature, the rigidly aggregated Fh nanoparticles agglomerate into large particles and lose their inherent physicochemical characteristics.[11,15] Other disadvantages that limit the use of Fhs in the treatment of contaminant gases are the lack of mesoporosity, low pore volume, and/or high vulnerability to phase transformation.[11,16]

We conjectured that the development of Fh-based materials with mesoporous structures and high surface areas would have the potential to mitigate these drawbacks. Mesostructured transition metal oxides would be highly expected because confining *d*-electrons to the thin walls between pores can impart unusual magnetic and electrical properties. Furthermore, the high internal pore surface area of mesoporous transition oxides, which is very important for a catalyst material intended for adsorption and subsequent transformation processes, could lead to novel catalytic properties.[16-21] The application of mesoporous materials in catalysis has been extensively reviewed.[22,23] Similar to the studies of magnetic properties in these materials, catalytic properties have been investigated after filling the pores of the mesoporous framework with a catalyst. Such catalysts have shown substantially high conversions of cyclohexane to cyclohexanol and cyclohexanone.[24]

Having readily accessible and reactive surface defect sites, a partially dehydroxylated mesoporous Fh would be expected to be an interesting system for adsorption and catalysis applications. The preparation of mesoporous-phase pure Fe oxides has been difficult,[25-27] which has been attributed, in part, to the multiplicity of Fe oxidation states, such as FeO, Fe_2O_3, and Fe_3O_4. Furthermore, Fe_2O_3 occurs in different phases (e.g., α-Fe_2O_3 and γ-Fe_2O_3), of which hematite, α-Fe_2O_3, is the most thermodynamically stable form. Mesoporous Fe oxide has been prepared by using either a soft template (e.g., block copolymers, cetyltrimethylammonium bromide (CTAB), dodecyl sulfate, alkyl amines) or a hard template (e.g., mesoporous silica, mesoporous C) in a solution-phase process that allows mesoporous transition metal oxides to form in a stable oxidation state in solution.[28] In the former case, the mesoporous solid is assembled around the soft template, whereas in the latter, the mesoporous transition metal oxide is formed within the pores of the template. Subsequently, both types of templates are dissolved. However, when the temperature range in which the target phase forms does not match the stability range of the template, the desired phase is not obtained.

Ciesla et al. described the synthesis of a mesoporous

Fe oxide material using hexadecylsulfonic acid as an anionic surfactant.[29] However, their report was limited to the as-synthesized sample, and no details were provided on the porosity of the product. There have only been a few reports of mesoporous Fe oxyhydroxide-surfactant composites to date.[30-33] Various *n*-alkyl sulfates ($C_nH_{2n+1}OSO_3Na$, where n = 14, 16, 18) and Fe salts have been used as precursors, and synthesis was achieved by the controlled precipitation and hydrolysis of aqueous Fe cations into self-assembled Fe/surfactant arrays. These composite materials, however, had lamellar structures that collapsed upon calcination. None of these reports discussed the porosity or the properties of the materials after heat treatment.

In yet another variation, the synthesis of a mesoporous Fe oxide with a wormhole-like morphology was achieved by a sonochemical synthesis using Fe(III) ethoxide as the inorganic precursor and CTAB as an organic structure-directing agent,[34] and the products were found to exhibit high Brunauer-Emmett-Teller (BET) surface areas (177 m^2/g after calcination at 250°C for 4 h and 94 m^2/g at 500°C). However, the preparation suffered several disadvantages, including the following: (i) the initially formed amorphous α-Fe_2O_3 was converted into catalytically less active γ-Fe_2O_3 upon heating; (ii) the Fe ethoxide precursor was rather expensive; (iii) the mesoporous bodies were inhomogeneously distributed, with a major pore size of 3.9 nm and a minor pore size of 7.5 nm; and (iv) the sonochemical method of preparation would not be convenient for the bulk production of materials. Mesostructured Fe oxides have also been prepared by the in situ formation of transition metal alkoxides as precursors and carboxylate or amine surfactants as templates.[35] However, heat treatment of the Fe oxides obtained by this method, even at temperatures as low as 150°C, caused the mesostructure to collapse.

The synthesis and properties of an ordered two-dimensional hexagonal mesoporous Fe oxide (2DMIO) with *P6mm* symmetry and a three-dimensional cubic mesoporous Fe oxide (3DMIO) with *Fm3m* symmetry have been reported using Fe(III) ethoxide as the precursor and decylamine as the template.[36] The ethanol-extracted as-synthesized 2DMIO and 3DMIO showed excellent BET specific surface areas of 340 and 610 m^2/g, respectively. However, the mesoporous structure was thermally stable only up to 250°C. The poor thermal stability of the product and the high precursor cost render this process commercially unviable.

Mesoporous forms of crystalline β-FeOOH (akaganeite) have been synthesized by the surfactant-assisted templating method of nanoparticle assembly using $FeCl_3$ as the precursor. Such templates as a cationic cetylpyridinium salt, an anionic dodecylsulfonate salt, or the nonionic polyoxyethylene(10) cetyl ether have been used.[37] However, the surface area of these materials decreased dramatically as the calcination temperature increased to 300°C. A sulfate- and phosphate-free mesostructured Fe oxide using the chelating triol surfactant 1,1,1-tris(hydroxymethyl)undecane has also been prepared.[38] However, upon calcination, the structure decomposed and crystallization of the mesophase resulted in the formation of maghemite. When this material was calcined at 400°C, the BET specific surface area decreased dramatically to 32 m^2/g.

The synthesis of ordered and disordered Fe oxides has been achieved using mesoporous silica and mesoporous carbon as hard templates.[39-41] Although Fe oxides with exact molds could be obtained, both surfactants and large amounts of the mesoporous template were consumed to obtain the final product, increasing the cost of the overall process. Using the well-defined mesopores of the rigid framework assembly of mesoporous silica, ordered and disordered mesoporous 2LFh were successfully prepared for the first time under calcination conditions, but a certain amount of Si was necessary to maintain the characteristic 2LFh phase.[42] The presence of the Si species modified the surface characteristics of Fh,[11,15b] with possible adverse effects on its catalytic performance.

To the best of our knowledge, there is no suitable synthesis strategy to date for producing mesoporous 2LFh that is free of Si and resistant to phase transformation, at least under moderate calcination conditions; consequently, the efficacy of mesoporous 2LFh in air purification and its intriguing physicochemical characteristics remain unexplored. Thus, it would be highly desirable to obtain stable, dehydrated Fh nanoparticles, preferably produced as a calcined material with a characteristic pore network in the mesopore regime, for air purification. Here, we present a solution-phase assembly process for producing mesoporous 2-line ferrihydrite (M2LFh),

which we found to be resistive to phase transition upon moderate calcination treatment and/or aging.[43] The M2LFh produced by this method was highly efficient in eliminating O_3 from air at RT. We will also illustrate that the coexistence of Fh nanoparticles and their relative proportion in disordered mesoporous Fe oxides play decisive roles in achieving high catalytic performance.[44] This is the first review in which the most important physicochemical characteristics of Fh are exploited for air purification applications.

2. Experimental

2. 1 Preparation of Mesoporous 2-line Ferrihydrite

M2LFh was synthesized by a precipitation-induced self-assembly using a suitable base and template.[43] Our synthesis strategy was to carry out the precipitation in a low-polarity solvent, preferably in an organic solvent with reduced H-bonding ability. The predominant formation of Fh nanoparticles with a limited amount of water on the particle surfaces and control of the solution-phase crystal growth were desirable to produce the targeted material. The following can be given as reasons. When surface metal cations with stable valence states (e.g., Fe^{3+}) cannot form stable surface complexes with the solvent (e.g., 1-propanol), association of the surface hydroxyl groups of the Fe hydroxide species with a surfactant through electrostatic or H-bonding interactions is not hindered by the solvent. In our case, owing to its relatively low H-bonding ability, 1-propanol does not interfere significantly with the interaction between iron hydroxide and the surfactant species. As a result, the Fh nanoparticles are stabilized in solution and self-assembly occurs. The initial selective formation of Fh can be considered an advantage as Fh is a poorly crystalline solid that is usually obtained as a high-surface-area nanoparticle powder in contrast to goethite, which readily agglomerates into large particles or crystallites.[45] Moreover, the alkyl polyoxyethylene template stabilizes the Fh nanoparticles through H-bonding. It has been documented that the presence of organic matter (both 1-propanol and the template in the present case) in the coordination sphere of Fh nanoparticles impedes the nucleation of primary particles and solution-phase crystal growth through a steric effect.[46] The combined use of a nonaqueous solvent medium and the template results in a cooperative effect that efficiently organizes the stabilized 2LFh nanoparticles into an assembly with a mesoporous structure. The interparticle mesoporous network established through this cooperative assembly process imparts extra stability to the 2LFh lattice by providing adequate separation between the particles. This prevents agglomeration of the nanoparticles and large particle growth during the elimination of structured water by moderate heat treatment. We therefore carried out a controlled precipitation of the Fe nitrate salt precursor in a nonaqueous solvent medium (1-propanol) using polyoxyethylene (20) cetyl ether (Brij 58) as a template. The preparation method is illustrated in **Fig. 1**.

For comparison, 2LFh was prepared according to a literature procedure.[10] Additionally, a mesostructured semicrystalline Fe oxide, in which amorphous Fh nanoparticles coexist with the γ-Fe_2O_3 phase (MSIO), and a crystalline Fe oxide with no well-defined mesopores (CIO) were prepared[44a] to compare gaseous O_3 decomposition. MSIO was prepared through a sol-gel process in which Fe nitrate, oleic acid, the triblock polymer template F-127 (Sigma-Aldrich), and 1-propanol were mixed, followed by aging and calcination. CIO was prepared by the self-assembly of Fe oxyhydroxide in a water-ethylene glycol mixture in the presence of CTAB (Kishida Chemical).

2. 2 Characterization

X-ray diffraction (XRD) patterns were obtained on a Rigaku Rint-2400 operated at 40 kV and 30 mA using Cu Kα radiation. Transmission electron microscopy (TEM) observations were performed using a JEM200CX (Hitachi) at an accelerating voltage of 200 kV. N_2 adsorption analysis was carried out on a BELSORP 18 (BEL Japan, Inc.). The Mössbauer spectra of ^{57}Fe were obtained using a constant-acceleration spectrometer with a ^{57}Co/Rh source at room temperature. The velocity scale was calibrated using the standard magnetic sextuplet signals of a pure iron foil absorber. All the spectra were deconvoluted with calculated Mössbauer spectra consisting of Lorentzian line shapes.

The Fe K-edge extended X-ray absorption fine structure (EXAFS) and X-ray absorption near-edge structure (XANES) measurements were performed using BL33XU at SPring-8 (Hyogo, Japan). The O K-edge near edge X-ray absorption fine structure

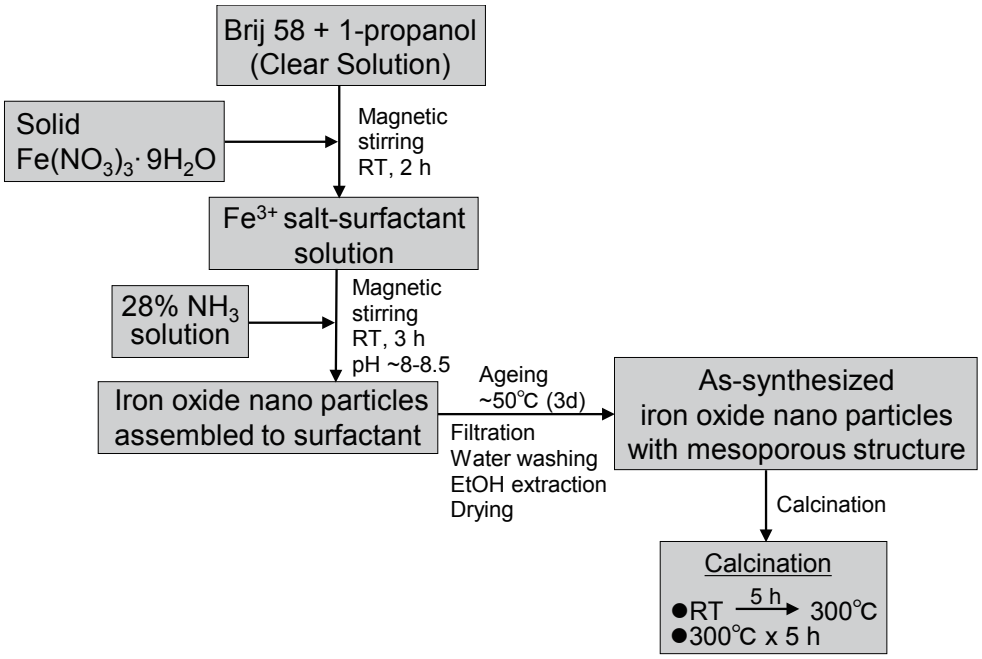

Fig. 1 A schematic illustration of the synthesis of M2LFh.

(NEXAFS) measurement was carried out using BL12 at SAGA-LS, Japan (1.4 GeV light source). The NEXAFS spectral measurements were obtained by the total-electron-yield (TEY) method.

The X-ray photoelectron spectroscopy XPS measurements were carried out on a Quantera SXM (Ulvac-PHI) spectrometer.

All surface structure calculations of Fh were carried out using density functional theory (DFT) with PWscf code.[47] The exchange correlation was treated by the generalized gradient approximation (GGA) of Perdew, Burke, and Ernzerhof (PBE).[48] We also utilized the GGA+U method to modify the GGA energies with an explicit correction for the Coulomb interaction of the 3d electrons of Fe.[49-51] Michel's defect-free single-phase structural model of Fh was used as the bulk model (structural formula: Fe_5O_8H; hexagonal space group: $P6_3mc$).[10] The optimized surface structure of Fh was used for O_3 adsorption calculations.

2. 3 O_3 Removal Analysis

The O_3 removal measurements were carried out on a fixed bed down-flow reactor filled with 0.2 g of catalyst with a pellet size of 0.5 mm. O_3 was generated by an electric discharge through O_2 under a suitable voltage. The resulting (O_2 + O_3) gas mixture at a flow rate of 0.5 L/min was mixed with N_2 gas at a flow rate of 4.5 L/min, for a total gas flow rate of 5 L/min. The electric discharge was adjusted so that the initial concentration of O_3 in the gas mixture was 600 ppm. The reactant gas mixture was passed over the catalyst, which was maintained at room temperature. The O_3 concentration was measured using a chemiluminescence method, in which residual O_3 was reacted with 1000 ppm NO. The O_3 conversion was calculated with respect to the initial concentration.

3. Results and Discussion

3. 1 Characterization of M2LFh

As evidenced by line (A) in **Fig. 2**, the wide-angle XRD pattern of M2LFh shows two broad reflections

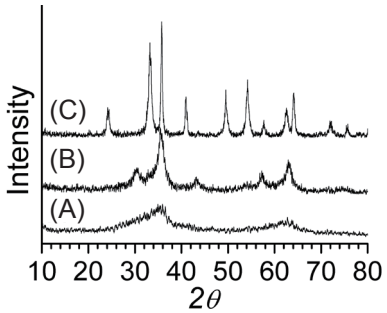

Fig. 2 Wide-angle XRD patterns of (A) M2LFh, (B) MSIO, and (C) CIO.

that are characteristic of the 2-line Fh phase. Although the amorphous Fh phase reflections in the XRD pattern of MSIO (line (B) in Fig. 2) are largely disguised by the crystalline peaks of γ-Fe_2O_3, the Mössbauer analysis estimates show that MSIO contains about 47% Fh and 53% γ-Fe_2O_3. In the case of CIO, all the diffraction peaks (line (C) in Fig. 2) are in good agreement with the standard XRD pattern of the hexagonal phase of α-Fe_2O_3 (JCPDS No. 80-2377), which the Mössbauer analysis corroborates. A broad, low-angle XRD peak is observed at 2θ = 0.5-3.0° (**Fig. 3**) for both M2LFh and MSIO, which is typical of disordered mesostructured materials. Further, the observation of a characteristic type-IV isotherm with a homogeneous pore size distribution in the range of 4-6 nm by N_2 adsorption analyses (**Fig. 4**) provides critical evidence that both M2LFh and MSIO are mesoporous. The absence of such characteristics suggests that CIO is non-mesoporous. The BET specific surface areas of M2LFh, MSIO, and CIO are 180, 140, and 82 m^2/g, respectively. The low-angle XRD results for M2LFh and MSIO are corroborated by the TEM images (**Fig. 5**), which illustrate the presence of a disordered mesoporous structure in both M2LFh and MSIO. In M2LFh, primary nanoparticles less than 10 nm in size aggregate into a disordered mesoporous structure. In the case of MSIO, a mixture of spherical and fibrous particles is apparent. In CIO, α-Fe_2O_3 is largely crystallized as tube-like particles several nanometers in length (< 500 nm) with irregular intraparticle pores. Scherrer analysis reveals that the wall structures of both MSIO and CIO are made up of particles with average crystallite sizes of about 8 and 18 nm, respectively. The selected-area electron diffraction (SAED) pattern of M2LFh is typical of 2-line Fh (Fig. 5(a), inset), whereas in MSIO, both Fh and γ-Fe_2O_3 phases were identified (not shown). The ring-type electron diffraction patterns of M2LFh and MSIO indicate the disordered nature of these materials. The strong electron diffraction spots in the SAED pattern of CIO further confirm that this material is largely crystallized as α-Fe_2O_3.

3. 2 O_3 Removal Ability

We studied O_3 removal at RT to evaluate the efficacy of these materials in comparison with other Fe materials and MnO_2, which has been reported to be the most active catalyst for the O_3 decomposition reaction. Among all the materials we tested at RT, M2LFh was found to be the most efficient candidate for O_3 decomposition, showing about 95% O_3 removal with high reproducibility (**Fig. 6**, Sample (A)). MSIO (Sample (B)) resulted in an O_3 conversion of 87%, whereas CIO (Sample (C)) showed 71% O_3 removal. The O_3 decomposition efficiencies of M2LFh and MSIO were also remarkably better than that of γ-Fe_2O_3 (Sample (E), 17.5 m^2/g, High Purity Chemicals) and microporous Fe incorporating 5 wt% Fe/ZSM-5 (Sample (F)), both of which showed less than 5% O_3 removal at RT. MnO_2 is used practically as a commercial catalyst for O_3 removal from equipment such as electrostatic copying machines.[5] In this study, a commercially available O_3 decomposition catalyst (Sample (G), MnO_2: CMD 200, 200 m^2/g, supplied by Chuo Denki Kagaku Kogyo) exhibits an O_3 conversion of only about 71%. In a previous study, we verified that

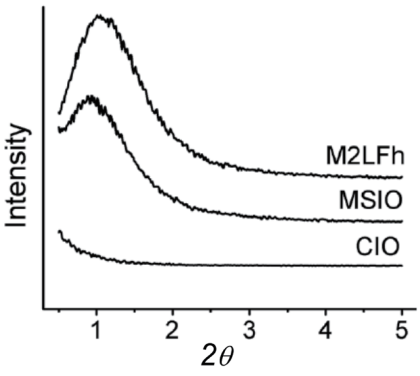

Fig. 3 Low-angle XRD patterns of M2LFh, MSIO, and CIO.

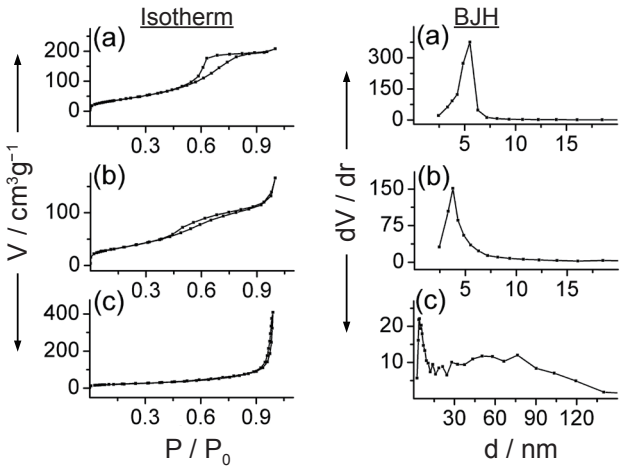

Fig. 4 The N_2 adsorption-desorption isotherms and the Barrett-Joyner-Halenda (BJH) analysis of pore size distribution for (a) M2LFh, (b) MSIO, and (c) CIO.

non-mesoporous 2LFh (Sample (D), 223 m^2/g) prepared by the conventional route[10] was less effective for O_3 removal than M2LFh, showing only 71% conversion at RT. This result pointed to the importance of the mesoporous structure and the absence of structured water in M2LFh. These features are advantageous for reducing constraints on the diffusion of gas molecules, which increases the interfacial reaction rate between O_3 and Fh nanoparticles.

The pivotal role of Fh nanoparticles in O_3 removal is evidenced by comparing the activities of γ-Fe_2O_3 (Sample (E)) and MSIO (Sample (B)), which is a mixture of γ-Fe_2O_3 and Fh (47% Fh by XRD). For example, MSIO (87% conversion) shows a conversion rate about 44 times higher than that of γ-Fe_2O_3 at RT.

We are convinced that the presence of mesopores and the physicochemical characteristics of Fh would be useful for the removal of other gases/reactants present in an air stream, such as in the ozonation process used for degradation of organic compounds, or during a reaction carried out in the presence of other reactant species, such as water vapor. Indeed, when the O_3 decomposition reaction was carried out with water vapor at 75°C, M2LFh showed a distinctly higher performance than other Fe materials.[44]

3. 3 Correlation between the Surface State and O_3 Removal Activity of M2LFh

We performed various X-ray absorption analyses of M2LFh, MSIO, and CIO to gain insight into the surface and bulk structural features of these materials and, hence, their influences on O_3 removal performance.

The EXAFS analysis of these samples shows a progressive softening of oscillations in the Fe K-edge spectra (**Fig. 7**, left panel) with increasing Fh amount in the sample. Thus, as the Fh contribution increases from CIO to M2LFh, a gradual decrease in peak

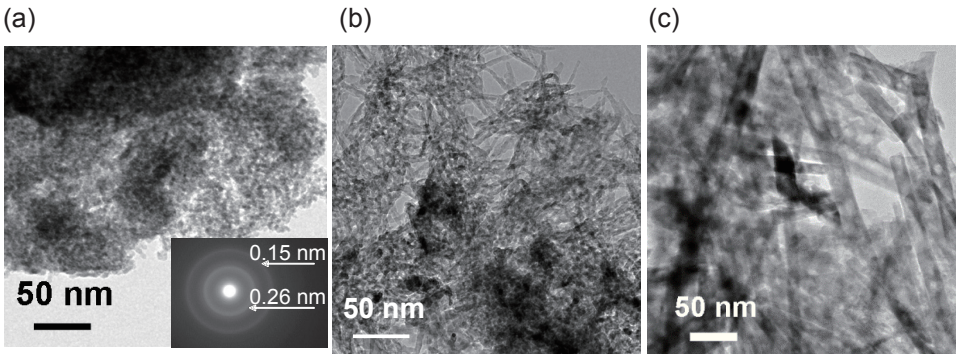

Fig. 5 TEM images of (a) M2LFh, (b) MSIO, and (c) CIO and SAED pattern(inset) of M2LFh.

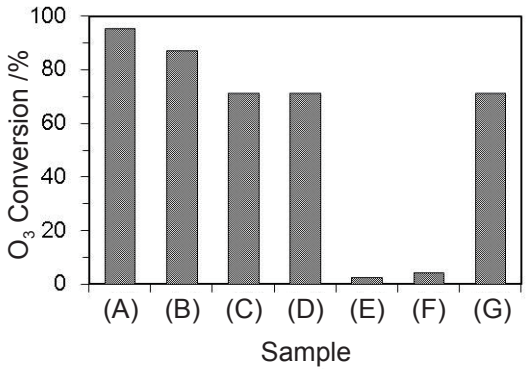

Fig. 6 Comparison of the O_3 removal performance of various samples at RT: (A) M2LFh, (B) MSIO, (C) CIO, (D) 2LFh, (E) γ-Fe_2O_3, (F) 5 wt% Fe/ZSM-5, and (G) MnO_2.

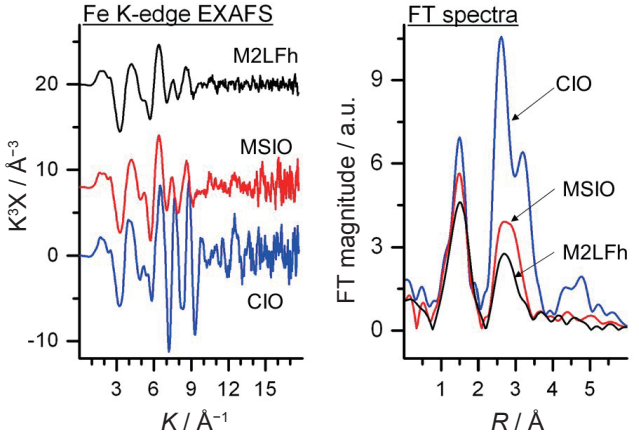

Fig. 7 The Fe K-edge EXAFS spectra (left panel) and the corresponding FT spectra (right panel of M2LFh (black), MSIO (red), and CIO (blue)).

intensity is observed in the corresponding Fourier transform (FT) spectra, particularly for the peak within the 2-4 Å range, which corresponds to the Fe-Fe distances (Fig. 7, right panel). This suggests that, in comparison with CIO, a long-range structural order is lacking in Fh materials,[43] which induces strain and thus variation in the local bonding environment, such as the specific symmetry and coordination number of the structural unit cell of these compounds.

XANES spectra of M2LFh, MSIO, and CIO at the Fe K-edge are presented in **Fig. 8**. The characteristic pre-edge peak observed in the spectra in all cases illustrates the presence of non-centrosymmetric Fe sites.[52] The pre-edge peak at around 7112 eV can be assigned to the 1s→3d dipole transition. This transition is usually a forbidden transition and stronger in compounds that are distorted from the octahedral shape, such as when a metal atom is in tetrahedral coordination. Among M2LFh, MSIO, and CIO, CIO with the α-Fe_2O_3 phase shows the lowest pre-edge peak intensity because the oxygen atoms in α-Fe_2O_3 are packed around Fe^{3+} with almost the same density, and thus cause only a slight distortion in the octahedral environment of Fe^{3+}.[53] The finding that the pre-edge peak intensities of M2LFh and MSIO are higher than that of CIO implies that the particle surfaces of M2LFh and MSIO are enriched with coordinately unsaturated Fe sites with a different symmetry and coordination number. This may arise due to the high surface areas and relatively smaller sized particles with many probable surface defects of Fh nanoparticles. In other words, the abundant unsaturated, coordinated Fe sites on the Fh particle surface affect the pre-edge peak feature and its intensity differently. We believe that the surface-enriched, unsaturated Fe sites in mesostructured Fh-based materials are readily available for adsorption and reaction. Thus, M2LFh having only the Fh phase shows the highest O_3 removal activity.

More information on the electronic states of these materials from the oxygen perspective was obtained by O K-edge NEXAFS spectroscopy, which is more surface-sensitive than both EXAFS and XANES (**Fig. 9**). The well-resolved splitting of Fe 3d states into t_{2g} and e_g symmetry bands in Region A (corresponding to Fe 3d + O 2p bands), as well as a relatively high peak intensity in Region B (corresponding to O 2p hybridized with Fe 4sp bands) are clear indications of the high packing density of oxygen atoms around the Fe atoms in CIO. In contrast, the splitting of the 3d state is not well-resolved for Fh materials, and appears as a broad peak with decreased intensity of the A′ peak feature. This is ascribed to the inherent convoluted splitting of Fe in different coordination environments with less closely packed atoms and highly isolated FeO_x species[53] in M2LFh and MSIO. These results agree with the EXAFS and XANES results.

Thus, the high activity of Fh-based materials is due to the abundantly available unsaturated surface Fe sites with relatively less dense oxygen packing around them and the presence of isolated FeO_x species. The presence of isolated FeO_x presumably renders M2LFh and MSIO more easily reducible than CIO and other crystalline Fe oxides, as revealed by TPR analysis with H_2,[44] thus, M2LFh and MSIO show the highest activity. This is in agreement with a previous study reporting that an easily reducible metal oxide is more

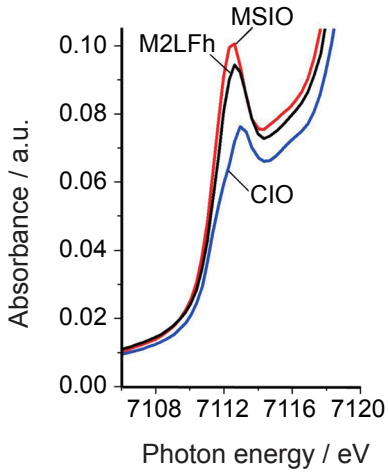

Fig. 8 The pre-edge peak from Fe K-edge XANES spectra of M2LFh (black), MSIO (red), and CIO (blue).

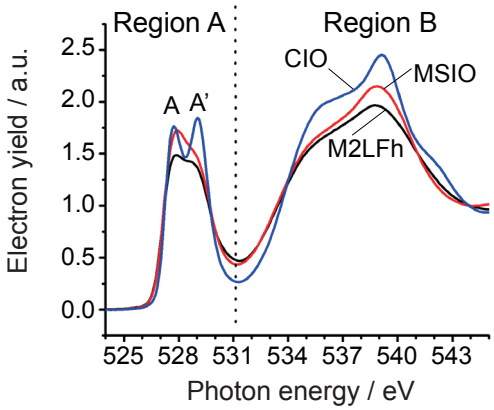

Fig. 9 The O K-edge NEXAFS spectra of M2LFh (black), MSIO (red), and CIO (blue).

active for O_3 decomposition.[6] Further, in the case of CIO, the relatively low peak intensity of the Fe 4sp + O 2p states (Fig. 9, Region B) and the reduced packing of oxygen around Fe sites indicate that the metallic electrons of M2LFh and MSIO are more localized around Fe atom sites. Thus, the Fe 3d + O 2p states with electrons more localized around the Fe atom sites can readily interact with electron-deficient O_3 molecules through both π and σ bonds. In contrast to M2LFh and MSIO, the relatively high peak intensity of the Fe 4sp + O 2p states of CIO suggests that a higher electron density is spread to the weakly structured Fe 4sp states in CIO. As the electron cloud in the Fe 4sp + O 2p states is less localized around the Fe atom sites, O_3 interaction with CIO leads to reduced overall charge transfer from its oxide surface to the O_3 molecule. Correspondingly, when the peak maxima of the Fe 4sp + O 2p states of these compounds and O_3 activity are plotted and expressed in terms of electron yield versus O_3 removal, it is clear that the activity decreases as the electron yield increases (**Fig. 10**). This suggests that CIO, with a highest contribution of Fe 4sp states, shows the lowest activity.

Finally, our DFT calculation reveals that the unsaturated Fe sites make the Fh surface enriched, which supports our EXAFS/XANES-based interpretation. Moreover, the interaction between O_3 and the Fh(110) surface was examined using DFT calculations based on the proposed M2LFh theoretical model for a fundamental understanding.[43] **Figs. 11**(a) and (b) illustrate the moieties of the most stable configuration on each adsorption site, and Figs. 11(c) and (d) depict the amount of electron transfer during O_3 adsorption. The amount of electron transfer was obtained through the integrated charge density difference ($\Delta\rho(r)$) for each atom in our calculation system.[44] The increasing flow of the electron density area (orange regions) could be recognized from the bonding formation between the O_3 terminal oxygen atom(s) and Fe sites, which could be understood as nucleophilic addition of O_3 to the active sites. We examined the amount of charge (electron transfer) by Löwdin charge population (LCP) analysis.[54] We found that the population of O 2p in O_3 increased from 4.26 to 4.59 at O (I) in mono-coordinated adsorption (*tri*-coordinated), and from 4.26 to 4.56 (4.50) at O (I, III) in bi-coordinated adsorption (*tetra*-coordinated). These results indicated that the charge transfer (O_3→Fh) was smaller than the back donation (Fh→O_3) during the adsorption scheme. The charge density analysis suggests that O_3 has a very strong tendency to adopt both monodentate and bidentate modes of adsorption on the Fh surface, which occurs on both Fe sites (*tri*-/*tetra*-coordinate).[44]

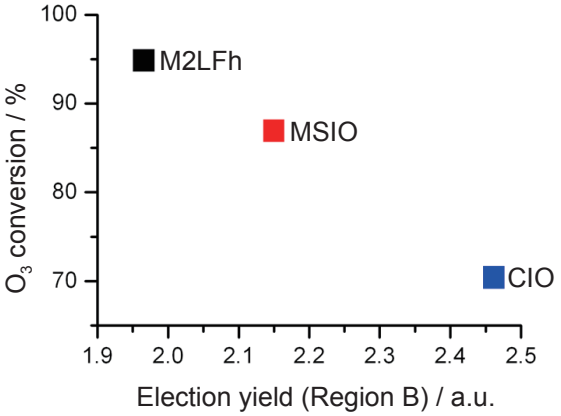

Fig. 10 A plot of electron yield obtained from the O K-edge NEXAFS peak maximum in the region B (corresponding to Fe 4sp + O 2p states) versus O_3 removal activity for each sample at RT. The activity decreases with relative increase of Fe 4sp contribution to the bonding.

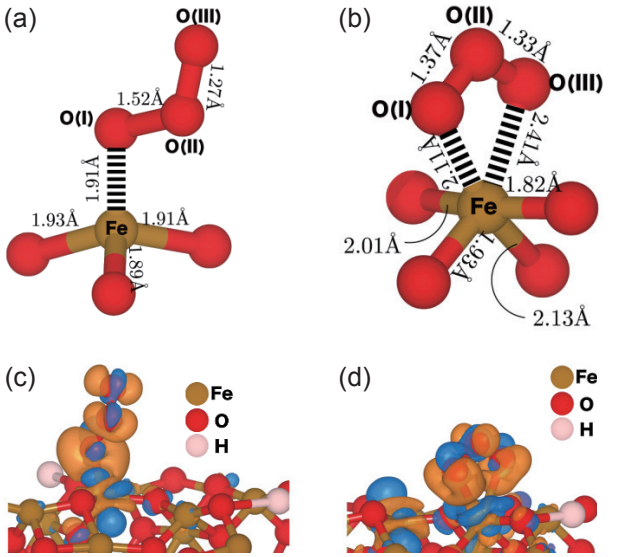

Fig. 11 (a) The partial structure derived from the optimized structure of O_3 adsorbed on Fh (110) *tri*-coordinated Fe site. (b) The partial structure derived from the optimized structure of O_3 adsorbed on Fh(110) *tetra*-coordinated iron site. (c), (d) Charge density difference for O_3 adsorbed on Fh(110). The charge flows from blue regions to orange regions. (c) O_3 adsorbed on Fh(110) *tri*-coordinated iron site, and (d) O_3 adsorbed on Fh(110) *tetra*-coordinated iron site.

Furthermore, the lengths of the O bonds in gas-phase O_3 (1.28 Å) are comparable to those in O_3 adsorbed on *tri*-coordinated sites. This shows that the O (I)–O (II) bond (1.52 Å) is more elongated and the O (II)–O (III) bond (1.27 Å) has more of a double bond character. In other words, O_3 has a strong tendency to dissociate over *tri*-coordinated sites, generating a reactive atomic 'O' and an O_2 molecule. In contrast, the *tetra*-coordinated O–O bond length (1.33-1.37 Å) is slightly elongated and O_3 deformation is less compared to the *tri*-coordinated sites.

Thus, it is possible that the adsorbed O_3 on the Fh surface, either as dissociatively adsorbed atomic 'O' on *tri*-coordinated Fe sites or as the more electron-rich O_3 on *tetra*-coordinated Fe sites, undergoes reaction with another coming O_3 molecule from the gaseous phase through an Eley-Rideal type scheme,[6] resulting in gaseous O_2 and reactive peroxide species adsorbed on the Fh surface.

4. Conclusions

We have demonstrated, for the first time, the exceptionally high activity of mesoporous Fh-based Fe oxides for O_3 removal at RT. Although we have tested a wide range of materials, none showed an O_3 removal performance as high as that of mesoporous ferrihydrite under the conditions employed here. Our study also showed the promise of the highly favorable textural and electronic structures of mesoporous Fh or Fh-based Fe oxides in environmental catalysis, especially for the removal of the noxious components in air under ambient reaction conditions. We believe that the characteristic mesoporous structure, which provides surface-enriched coordinatively unsaturated Fe sites, and the highly dehydrated surface, which provides accessible pathways for guest molecule entry, are the main factors contributing the high catalytic activity. Given the ambiguity surrounding the exact nature of the Fh surface, a fascinating outcome of the present investigation is that by examining the catalytic and adsorption behavior of the highly polarizable O_3 molecule on Fh nanoparticles, it is possible to obtain greater insight into the fine surface structure of Fh. We expect that our study will be of interest to a wide audience and trigger further work towards applications, as well as other fundamental research.

References

(1) a) Jenkin, M. E. and Clemitshaw, K. C., "Ozone and Other Secondary Photochemical Pollutants: Chemical Processes Governing Their Formation in the Planetary Boundary Layer", *Atmos. Environ*., Vol. 34, No. 16 (2000), pp. 2499-2527;
b) Nicolas, M., Ramalho, O. and Maupetit, F., "Reactions between Ozone and Building Products: Impact on Primary and Secondary Emissions", *Atmos. Environ*., Vol. 41, No. 15 (2007), pp. 3129-3138;
c) Zhang, J., Lioy, P. J. and He, Q., "Characteristics of Aldehydes: Concentrations, Sources, and Exposures for Indoor and Outdoor Residential Microenvironments", *Environ. Sci. Technol*., Vol. 28, No. 1 (1994), pp. 146-152.

(2) a) Booker, F., Muntifering, R., McGrath, M., Burkey, K., Decoteau, D., Fiscus, E., Manning, W., Krupa, S., Chappelka, A. and Grantz, D., "The Ozone Component of Global Change: Potential Effects on Agricultural and Horticultural Plant Yield, Product Quality and Interactions with Invasive Species" , *J. Integr. Plant Biol.*, Vol. 51, No. 4 (2009), pp. 337-351;
b) Hubbell, B. J., Hallberg, A., McCubbin, D. R. and Post, E., "Health-related Benefits of Attaining the 8-Hr Ozone Standard", *Environ. Health Perspect*., Vol. 113, No. 1 (2005), pp. 73-82.

(3) a) Centi, G., Ciambelli, P., Perathoner, S. and Russo, P., "Environmental Catalysis: Trends and Outlook", *Catal. Today*, Vol. 75, No. 1-4 (2002), pp. 3-15;
b) Zwinkels, M. F. M., Jaras, S. G. and Menon, P. G., "Catalytic Materials for High-temperature Combustion", *Catal. Rev. Sci. Eng*., Vol. 35, No. 3 (1993), pp. 319-358.

(4) a) Sinha, A. K. and Suzuki, K., "Three-dimensional Mesoporous Chromium Oxide: A Highly Efficient Material for the Elimination of Volatile Organic Compounds", *Angew. Chem. Int. Ed*., Vol. 44, No. 2 (2005), pp. 271-273;
b) "Cleaning up the Air" (Research Highlight), *Nat. Mater*., Vol. 4, No. 3 (2005), p. 187;
c) Suzuki, K. and Sinha, A. K., "Monodisperse, Bimodal Mesoporous Ceria Catalysts and Adsorbents for Air Purification", *J. Mater. Chem*., Vol. 17, No. 24 (2007), pp. 2547-2551;
d) Sinha, A. K., Suzuki, K., Takahara, M., Azuma, H., Nonaka, T. and Fukumoto, K., "Mesostructured Manganese Oxide/Gold Nanoparticle Composites for Extensive Air Purification", *Angew. Chem. Int. Ed*., Vol. 46, No. 16 (2007), pp. 2891-2894.

(5) Dhandapani, B. and Oyama, S. T., "Gas Phase Ozone Decomposition Catalysts", *Appl. Catal. B*, Vol. 11, No. 2 (1997), pp. 129-166.

(6) Li, W., Gibbs, G. V. and Oyama, S. T., "Mechanism of Ozone Decomposition on a Manganese Oxide Catalyst. 1. In Situ Raman Spectroscopy and Ab Initio Molecular Orbital Calculations", *J. Am. Chem. Soc*.,

Vol. 120, No. 35 (1998), pp. 9048-9046.
(7) Lin, J., Kawai, A. and Nakajima, T., "Effective Catalysts for Decomposition of Aqueous Ozone", *Appl. Catal. B*, Vol. 39, No. 2 (2002), pp. 157-165.
(8) Subrahmanyam, C., Bulushev, D. A. and Kiwi-Minsker, L., "Dynamic Behaviour of Activated Carbon Catalysts during Ozone Decomposition at Room Temperature", *Appl. Catal. B*, Vol. 61, No. 1-2 (2005), pp. 98-106.
(9) Cornell, R. M. and Schwertmann, U., *The Iron Oxides: Structure, Properties, Reactions, Occurrence and Uses* (1996), 573p., John Wiley & Sons, Inc.
(10) Michel, F. M., Ehm, L., Antao, S. M., Lee, P. L., Chupas, P. J., Liu, G., Strongin, D. R., Schoonen, M. A. A., Phillips, B. L. and Parise, J. B., "The Structure of Ferrihydrite, a Nanocrystalline Material", *Science*, Vol. 316, No. 22 (2007), pp. 1726-1729.
(11) Jambor, J. L. and Dutrizac, J. E., "Occurrence and Constitution of Natural and Synthetic Ferrihydrite, a Widespread Iron Oxyhydroxide", *Chem. Rev*., Vol. 98. No. 7 (1998), pp. 2549-2586.
(12) a) Keppler, F., Eiden, R., Niedan, V., Pracht, J. and Schöler, H. F., "Halocarbons Produced by Natural Oxidation Processes during Degradation of Organic Matter", *Nature*, Vol. 403, No. 20 (2000), pp. 298-301;
b) Hochella Jr., M. F., Lower, S. K., Maurice, P. A., Penn, R. L., Sahai, N., Sparks, D. L. and Twining, B. S., "Nanominerals, Mineral Nanoparticles, and Earth Systems", *Science*, Vol. 319, No. 21 (2008), pp. 1631-1635;
c) Beal, E. J., House, C. H. and Orphan, V. J., "Manganese- and Iron-dependent Marine Methane Oxidation", *Science*, Vol. 325, No. 10 (2009), pp, 184-187.
(13) Machala, L., Zboril, R. and Gedanken, A., "Amorphous Iron(III) Oxide – A Review", *J. Phys. Chem. B*, Vol. 111, No. 16 (2007), pp. 4003-4018.
(14) Erbs, J. J., Gilbert, B. and Penn,R. L., "Influence of Size on Reductive Dissolution of Six-line Ferrihydrite", *J. Phys. Chem. C*, Vol. 112, No. 32 (2008), pp. 12127-12133.
(15) a) Feng, Z., Zhao, J., Huggins, F. E. and Huffman, G. P., "Agglomeration and Phase Transition of a Nanophase Iron Oxide Catalyst", *J. Catal.*, Vol. 143, No. 2 (1993), pp. 510-519;
b) Zhao, J., Huggins, F. E., Feng, Z. and Huffman, G. P., "Ferrihytdrite: Surface Structure and Its Effects on Phase Transformation", *Clays and Clay Minerals*, Vol. 42, No. 6 (1994), pp. 737-746;
c) Lewis, D. G., "Transformations Induced in Ferrihydrite by Oven-drying", *J. Plant. Nutr. Soil. Sci.*, Vol. 155, No. 5 (1992), pp. 461-466;
d) Ristić, M., De Grave, E., Musić, S., Popović, S. and Orehovec, Z., "Transformation of Low Crystalline Ferrihydrite to α-Fe_2O_3 in the Solid State", *J. Mol. Struct.*, Vol. 834, No. 27 (2007), pp. 454-460.
(16) Antonelli, D. M. and Ying, J. Y., "Synthesis of Hexagonally Packed Mesoporous TiO_2 by a Modified Sol – Gel Method", *Angew. Chem., Int. Ed*., Vol. 34, No. 18 (1995), pp. 2014-2017.
(17) Schüth, F., "Non-siliceous Mesostructured and Mesoporous Materials", *Chem. Mater*., Vol. 13, No. 10 (2001), pp. 3184-3195.
(18) Yang, P., Deng, T., Zhao, D., Feng, P., Pine, D., Chmelka, B. F., Whitesides, G. M. and Stucky, G. D., "Hierarchically Ordered Oxides", *Science*, Vol. 282, No. 5397 (1998), pp. 2244-2246.
(19) He, X. and Antonelli, D., "Recent Advances in Synthesis and Applications of Transition Metal Containing Mesoporous Molecular Sieves", *Angew. Chem., Int. Ed*., Vol. 41, No. 2 (2002), pp. 214-229.
(20) Behrens, P., "Voids in Variable Chemical Surroundings: Mesoporous Metal Oxides", *Angew. Chem., Int. Ed*., Vol. 35, No. 5 (1996), pp. 515-518.
(21) Huo, Q. S., Margolese, D. I., Ciesla, U., Demuth, D. G., Feng, P. Y., Gier, T. E., Sieger, P., Firouzi, A., Chmelka, B. F., Schuth, F. and Stucky, G. D., "Organization of Organic Molecules with Inorganic Molecular Species into Nanocomposite Biphase Arrays", *Chem. Mater*., Vol. 6, No. 8 (1994), pp. 1176-1191.
(22) Yin, J. Y., Mehnert, C. P. and Wong, M. S., "Synthesis and Applications of Supramolecular-templated Mesoporous Materials", *Angew. Chem. Int. Ed*., Vol. 38, No. 1-2 (1999), pp. 56-77.
(23) Carma, A., "From Microporous to Mesoporous Molecular Sieve Materials and Their Use in Catalysis", *Chem. Rev*., Vol. 97, No. 6 (1997), pp. 2373-2420.
(24) Perkas, N., Wang, Y. Q., Koltypin, Y., Gedanken, A. and Chandrasekaran, S., "Mesoporous Iron-titania Catalyst for Cyclohexane Oxidation", *Chem. Commun*., Vol. 11, No. 11 (2001), pp. 988-989.
(25) Vollath, D., Szabo, D. V., Taylor, R. D., Willis, J. O. and Sickafus, K. E., "Synthesis and Properties of Nanocrystalline Superparamagnetic γ-Fe_2O_3", *Nanostruct. Mater*., Vol. 6, No. 5-8 (1995), pp. 941-944.
(26) Morales, M. P., Pecharroman, C., Gonzales, C. T. and Serna, C., "Structural Characteristics of Uniform γ-Fe_2O_3 Particles with Different Axial (Length/Width) Ratios", *J. Solid State Chem*., Vol. 108, No. 1 (1994), pp. 158-163.
(27) Kroll, E., Winnik, F. M. and Ziolo, R., "In Situ Preparation of Nanocrystalline γ-Fe_2O_3 in Iron(II) Cross-linked Alginate Gels", *Chem. Mater.*, Vol. 8, No. 8 (1996), pp. 1594-1596.
(28) Brezesinski, T., Groenewolt, M., Antonietti, M. and Smarsly, B., "Crystal-to-crystal Phase Transition in Self-assembled Mesoporous Iron Oxide Films", *Angew Chem., Int. Ed*., Vol. 45, No. 5 (2006), pp. 781-784.
(29) Ciesla, U., Demuth, D., Leon, R., Petroff, P., Stucky, G., Unger, K. and Schuth, F., "Surfactant Controlled Preparation of Mesostructured Transition-metal Oxide Compounds", *J. Chem. Soc., Chem. Commun*., No. 11

(1994), pp. 1387-1388
(30) Tolbert, S. H., Sieger, P., Stucky, G. D., Aubin, S. M. J., Wu, C.-C. and Hendrickson, D. N., "Control of Inorganic Layer Thickness in Self-assembled Iron Oxide/surfactant Composites", *J. Am. Chem. Soc*., Vol. 119, No. 37 (1997), pp. 8652-8661.
(31) Wirnsberger, G.,Gatterera, K. and Behrens, P., "Novel Synthetic Pathways to Layered Iron (hydro) Oxyhydroxide-surfactant Composites", *J. Mater. Chem*., Vol. 8, No. 7 (1998), pp. 1509-1510.
(32) Wirnsberger, G., Gatterer, K., Fritzer, H. P., Grogger, W., Pillep, B., Behrens, P., Hansen, M. F. and Koch, C. B., "Mesostructured Iron Oxyhydroxides. 1. Synthesis, Local Structure, and Magnetism", *Chem. Mater*., Vol. 13, No. 5 (2001), pp. 1453-1466.
(33) Wirnsberger, G., Gatterer, K., Fritzer, H. P., Grogger, W., Pillep, B., Behrens, P., Hansen, M. F. and Koch, C. B., "Mesostructured Iron Oxyhydroxides. 2. Soft Hydrothermal Restructuring Processes", *Chem. Mater*., Vol. 13, No. 5 (2001), pp. 1467-1472.
(34) Srivastava, D. N., Perkas, N., Gedanken, A. and Felner, I., "Sonochemical Synthesis of Mesoporous Iron Oxide and Accounts of Its Magnetic and Catalytic Properties", *J. Phys. Chem. B*, Vol. 106, No. 8 (2002), pp. 1878-1883.
(35) Malik, A.-S., Duncan, M. J. and Bruce, P. G., "Mesostructured Iron and Manganese Oxides", *J. Mater. Chem*., Vol. 13, No. 9 (2003), pp. 2123-2126.
(36) Jiao, F. and Bruce, P. G., "Two- and Three-dimensional Mesoporous Iron Oxides with Microporous Walls", *Angew. Chem. Int. Ed*., Vol. 43, No. 44 (2004), pp. 5958-5961.
(37) Yuan, Z.-Y., Ren, T.-Z. and Su, B.-L., "Surfactant Mediated Nanoparticle Assembly of Catalytic Mesoporous Crystalline Iron Oxide Materials", *Catal. Today*, Vol. 93-95 (2004), pp. 743-750.
(38) Lezau, A., Trudeau, M., Tsoi, G. M., Wenger, L. E. and Antonelli, D.,"Mesostructured Fe Oxide Synthesized by Ligand-assisted Templating with a Chelating Triol Surfactant", *J. Phys. Chem. B*, Vol. 108, No. 47 (2004), pp. 5211-5216.
(39) Jiao, F., Jumas, J.-C., Womes, M., Chadwick, A. V., Harrison, A. and Bruce, P. G., "Synthesis of Ordered Mesoporous Fe_3O_4 and γ-Fe_2O_3 with Crystalline Walls Using Post-template Reduction/oxidation", *J. Am. Chem. Soc*., Vol. 128, No. 39 (2006), pp. 12905-12909.
(40) Jiao, F., Harrison, A., Jumas, J.-C., Chadwick, A. V., Kockelmann, W. and Bruce, P. G., "Ordered Mesoporous Fe_2O_3 with Crystalline Walls", *J. Am. Chem. Soc*., Vol. 128, No. 16 (2006), pp. 5468-5474.
(41) Dong, X., Chen, H., Zhao, W., Li, X. and Shi, J., "Synthesis and Magnetic Properties of Mesostructured γ-Fe_2O_3/carbon Composites by a Co-casting Method", *Chem. Mater*., Vol. 19, No. 14 (2007), pp. 3484-3490.
(42) Tüysüz, H., Salabasü, E. L., Weidenthaler, C. and Schüth, F., "Synthesis and Magnetic Investigation of Ordered Mesoporous Two-line Ferrihydrite", *J. Am. Chem. Soc*., Vol. 130, No. 1 (2008), pp. 280-287.
(43) Mathew, T., Suzuki, K., Nagai, Y., Nonaka, T., Ikuta, Y., Takahashi, N., Susuki, N. and Shinjoh, H., "Mesoporous 2-line Ferrihydrite by a Solution-phase Cooperative Assembly Process for Removal of Organic Contaminants in Air", *Chem. Eur. J*., Vol. 17, No. 4 (2011), pp. 1092-1095.
(44) a) Mathew, T., Suzuki, K., Ikuta, Y., Nagai, Y., Nonaka, T., Takahashi, N. and Shinjoh, H., "Mesoporous Ferrihydrite-based Iron Oxide Nanoparticles as Highly Promising Materials for Ozone Removal", *Angew. Chem., Int. Ed*., Vol. 50, No. 32 (2011), pp. 7381-7384. ;
b) Suzuki, K. and Nagai, Y., "Mesoporous Ferrihydrite by a Solution-phase Cooperative Assembly Process for Air Purification", *Ceramics Japan* (in japanese), Vol. 49, No. 6 (2014), pp. 473-477.
(45) Khaleel, A. A., "Nanostructured Pure γ-Fe_2O_3 via Forced Precipitation in an Organic Solvent", *Chem. Eur. J*., Vol. 10, No. 4 (2004), pp. 925-932.
(46) Eusterhues , K., Wagner, F. E., Häusler, W., Hanzlik, M., Knicker, H., Totsche, K. U., Kögel-Knabner, I. and Schwertmann, U., "Characterization of Ferrihydrite-soil Organic Matter Coprecipitates by X-ray Diffraction and Mössbauer Spectroscopy", *Environ. Sci. Technol*., Vol. 42, No. 2 (2008), pp. 7891-7897.
(47) Giannozzi1, P., Baroni1, S., Bonini, N, Calandra, M., Car, R., Cavazzoni, C., Ceresoli, D., Chiarotti, G. L., Cococcioni, M., Dabo, I., Dal Corso, A., de Gironcoli1, S., Fabris, S., Fratesi, G., Gebauer, R., Gerstmann, U., Gougoussis, C., Kokalj, A., Lazzeri, M., Martin-Samos, L., Marzari, N., Mauri, F., Mazzarello, R., Paolini, S., Pasquarello, A., Paulatto, L., Sbraccia, C., Scandolo, S., Sclauzero, G., Seitsonen, A. P., Smogunov, A., Umari, P. and Wentzcovitch, R. M., "Quantum ESPRESSO: A Modular and Open-source Software Project for Quantum Simulations of Materials", *J. Phys.: Condens. Matter*., Vol. 21, No. 39 (2009), 395502.
(48) Perdew, J., Burke, K. and Ernzerhof, M., "Generalized Gradient Approximation Made Simple", *Phys. Rev. Lett*., Vol. 77, No. 18 (1996), pp. 3865-3868.
(49) a) Anisimov, V. I., Zaanen, J. and Andersen, O. K., "Band Theory and Mott Insulators: Hubbard *U* Instead of Stoner *I* ", *Phys. Rev. B*, Vol. 44, No. 3 (1991), pp. 943-954;
b) Liechtenstein, A. I., Anisimov, V. I. and Zaanen, J., "Density-functional Theory and Strong Interactions: Orbital Ordering in Mott-hubbard Insulators", *Phys. Rev. B*, Vol. 52, No. 8 (1995), pp. R5467-R5470.
(50) Pinney, N., Kubicki, J. D., Middlemiss, D. S., Grey, C. P. and Morgan, D., "Density Functional Theory Study of Ferrihydrite and Related Fe-oxyhydroxides", *Chem. Mater*., Vol. 21, No. 24 (2009), pp. 5727-5742.
(51) Rollmann, G., Entel, P., Rohrbach, A. and Hafner, J., "High-pressure Characteristics of α-Fe_2O_3 Using

DFT + *U*", *Phase Transitions*, Vol. 78, No. 1-3 (2005), pp. 251-258.
(52) Chen, L. X., Liu, T., Thurnauer, M. C., Csencsits, R. and Rajh, T., "Fe_2O_3 Nanoparticle Structures Investigated by X-ray Absorption Near-edge Structure, Surface Modifications, and Model Calculations", *J. Phys. Chem. B*, Vol. 106, No. 34 (2002), pp. 8539-8546.
(53) Park, T.-J., Sambasivan, S., Fischer, D. A., Yoon, W.-S., Misewich, J. A. and Wong, S. S., "Electronic Structure and Chemistry of Iron-based Metal Oxide Nanostructured Materials: A NEXAFS Investigation of $BiFeO_3$, $Bi_2Fe_4O_9$, α-Fe_2O_3, γ-Fe_2O_3, and Fe/Fe_3O_4", *J. Phys. Chem. C*, Vol. 112, No. 28 (2008), pp. 10359-10369.
(54) Sanchez-Portal, D., Artacho, E. and Soler, J. M., "Projection of Plane-wave Calculations into Atomic Orbitals", *Solid State Commun.,* Vol. 95, No. 10 (1995), pp. 685-690.

Figs. 2-11
Reprinted from Angew. Chem. Int. Ed., Vol. 50, No. 32 (2011), pp. 7381-7384, Mathew, T., Suzuki, K., Ikuta, Y., Nagai, Y., Nonaka, T., Takahashi, N. and Shinjoh, H., Mesoporous Ferrihydrite-based Iron Oxide Nanoparticles as Highly Promising Materials for Ozone Removal, © 2011 Wiley-VCH, with permission from John Wiley and Sons.

Kenichirou Suzuki
Research Field:
- Environmental Catalytic Chemistry
Academic Degree: Dr.Eng.